

# Magnetism in Quasi-One-Dimensional $A_2Cr_3As_3$ ( $A=K,Rb$ ) superconductors

Xianxin Wu,<sup>1</sup> Congcong Le,<sup>1</sup> Jing Yuan,<sup>1</sup> Heng Fan,<sup>1,2</sup> and Jiangping Hu<sup>1,3,2,\*</sup>

<sup>1</sup>*Institute of Physics, Chinese Academy of Sciences, Beijing 100190, China*

<sup>2</sup>*Collaborative Innovation Center of Quantum Matter, Beijing, China*

<sup>3</sup>*Department of Physics, Purdue University, West Lafayette, Indiana 47907, USA*

(Dated: April 22, 2015)

We predict that the recently discovered quasi-one dimensional superconductors,  $A_2Cr_3As_3$  ( $A=K,Rb$ ), possess strong frustrated magnetic fluctuations and are nearby a novel in-out co-planar magnetic ground state. The frustrated magnetism is very sensitive to c-axis lattice constant and can thus be suppressed by increasing pressure. Our results qualitatively explain strong non-Fermi liquid behaviors observed in the normal state of the superconductors as the intertwining between the magnetism and superconductivity can create a large quantum critical region in quasi-one dimensional systems and also suggest that the materials share similar phase diagrams and superconducting mechanism with other unconventional superconductors, such as cuprates and iron-based superconductors.

PACS numbers: 74.70.-b, 74.25.Ha, 74.20.Pq, 74.20.Rp

One of major challenges in condensed matter physics is to understand the role of electron-electron correlation in unconventional superconductors. The effect of electron-electron interaction becomes more important as the dimension of a system is lowered. Indeed, many unconventional superconductors discovered in the past are quasi-two dimensional(Q2D) electron systems. The superconductivity in these unconventional superconductors appears in a vicinity to a magnetically ordered state. Magnetic fluctuations which are caused by electron-electron interaction have been widely considered to be responsible for superconductivity and many non-Fermi liquid behaviors in normal states.

While there are many representatives of Q2D unconventional superconductors, it has been difficult to find one in quasi-one dimensional(Q1D) systems even if the effect of the electron-electron correlation is expected to be enhanced further. The Q1D superconductors discovered previously, including Bechgaard salts[1, 2],  $Tl_2Mo_6Se_6$ [3] and  $Li_{0.9}Mo_6O_{17}$ [4–7], are not attributed to 3d-orbital electrons which can exhibit strong electron-electron interaction.

Very recently, two novel Q1D materials  $K_2Cr_3As_3$ [8] and  $Rb_2Cr_3As_3$ [9] have been synthesized and found to be superconducting below the transition temperature 6.1 K and 4.8 K respectively. The structure of  $A_2Cr_3As_3$  ( $A=K,Rb$ ) is characterized by one-dimensional ( $Cr_3As_3$ ) chains (Fig.1(a)), which contain  $Cr_6$  distorted octahedral clusters. The alkali metal ions are intercalated between the ( $Cr_3As_3$ ) chains. Both new materials show strong non-fermi liquid behaviors in normal states, as well as unconventional superconducting properties in superconducting (SC) states. Moreover, just like cuprates and iron-based superconductors, the electronic physics in these new materials are likely attributed to 3d-orbitals of Cr atoms. Therefore the material may exhibit strong magnetism and electron-electron interaction.

In this paper, we show that the new materials can be a critical representative of Q1D unconventional superconductors

where the superconductivity emerges in a vicinity to a novel magnetically ordered state. We predict that the materials are characterized by strong frustrated magnetic fluctuations and are nearby a novel in-out co-planar(IOP) magnetic ground state. The magnetism can be described by a minimum effective model with three magnetic exchange parameters: the antiferromagnetic  $J_1$  and  $J'_1$  between two nearest-neighbor (NN) Cr atoms and the ferromagnetic  $J_2$  between two next NN Cr atoms along c-axis. The frustrated magnetism is very sensitive to c-axis lattice constant and can thus be suppressed by increasing pressure. The results suggest that the materials host a typical phase diagram similar to those of the Q2D unconventional superconductors, such as cuprates[10] and iron-based superconductors[11]. The new materials can be ideal systems to study the intimate relations between magnetism and superconductivity since a Q1D model can be solved theoretically with high controllability.

It is known that calculations based on the Density Functional Theory (DFT) can successfully identify the possible magnetic ground state in some correlated electron systems. Typical examples are the iron-based superconductors where theoretical calculations consistently agree well with experimental measurements[12–18] even if the magnetic origin is still debatable[19]. Here, we deploy similar DFT calculations. Our DFT calculations employ the projector augmented wave (PAW) method encoded in Vienna *ab initio* simulation package(VASP) [20–22], and generalized-gradient approximation (GGA)[23] for the exchange correlation functional is used. Throughout this work, the cutoff energy of 450 eV is taken for expanding the wave functions into plane-wave basis. The number of these  $k$  points are  $6 \times 6 \times 13$  for  $K_2Cr_3As_3$  and  $Rb_2Cr_3As_3$ [24]. The GGA plus on-site repulsion  $U$  method (GGA+ $U$ ) in the formulation of Dudarev *et al.*[25] is employed to describe the electron correlation effect associated with the Cr  $3d$  states by an effective parameter  $U_{eff}$ . The values of  $U=2.3$  eV and  $J=0.96$  eV on Cr are adopted for our GGA+ $U$  calculations[26]. We relax the lattice constants and internal atomic positions, where the plane wave cutoff energy is 600 eV. Forces are minimized to less than 0.01 eV/Å in the structural relaxation.

\*Electronic address: [jphu@iphy.ac.cn](mailto:jphu@iphy.ac.cn)

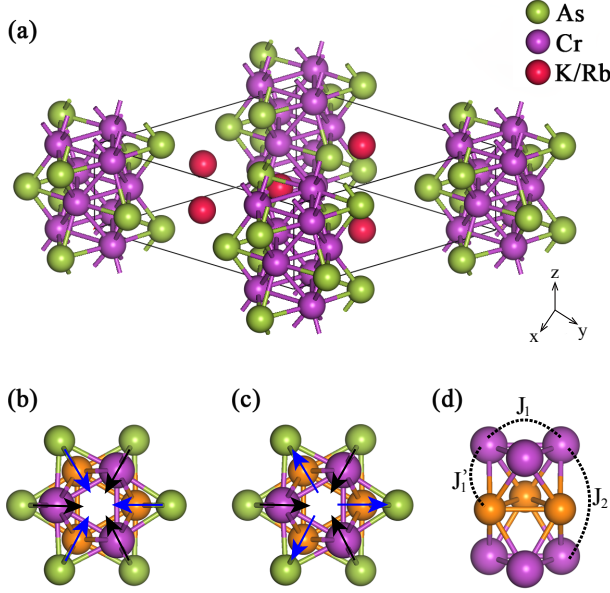


FIG. 1: Schematic view of the structure of  $A_2Cr_3As_2$  (a). (b) and (c) show the all-in and in-out noncollinear magnetic states. The exchange coupling parameters  $J_1$ ,  $J_1'$  and  $J_2$  are defined in (d). The orange and purple spheres represent Cr1 and Cr2.

TABLE I: Experimental and optimized structural parameters of  $K_2Cr_3As_3$  using GGA in the paramagnetic phase. Deviations between the optimized and experimental values are given in parentheses in %.

	GGA	EXP
$a(\text{\AA})$	10.113(+1.3)	9.983
$c(\text{\AA})$	4.147(-1.98)	4.230
Cr1-Cr1/Cr2-Cr2( $\text{\AA}$ )	2.498; 2.588	2.615; 2.691
Cr1-As1/Cr2-As2( $\text{\AA}$ )	2.513; 2.494	2.51; 2.49
Cr1-As2/Cr2-As1( $\text{\AA}$ )	2.522; 2.506	2.516; 2.506
$\alpha_1/\alpha_2(^{\circ})$	59.6; 62.51	62.8; 65.4
$\beta_1/\beta_2(^{\circ})$	60.8; 60.87	62.8; 62.9
$\gamma_1/\gamma_2(^{\circ})$	110.6; 111.6	114.4; 115.2

Due to the asymmetric distribution of alkali metal ions and the absence of inversion symmetry, there are two kinds of Cr ions in  $K_2Cr_3As_3$  ( $Rb_2Cr_3As_3$ ): Cr1 and Cr2. The Cr1 ions are surrounded by six inplane A ions and the inplane bondlength is 2.615(2.57) $\text{\AA}$ . The Cr2 ions are surrounded by three inplane alkali ions and the inplane bondlength is a bit longer, 2.69(3.16) $\text{\AA}$ . From the number of A ions surrounding Cr ions, it is expected that the Cr1As layer will obtain more electrons than the Cr2As layer.

The optimized and experimental structural parameters of  $K_2Cr_3As_3$  are summarized in Table I. We find that the lattice constants are comparable with experimental values but the Cr-Cr bond lengths are underestimated by 0.1  $\text{\AA}$ . Thus, the Cr1-As1-Cr1( $\alpha_1$ )/Cr2-As2-Cr2( $\alpha_2$ ), Cr1-As1-Cr2( $\beta_1$ )/Cr2-As2-Cr1( $\beta_2$ ) and Cr1-As2-Cr1( $\gamma_1$ )/Cr2-As1-Cr2( $\gamma_2$ ) angles are also underestimated. Similar cases have been also noted in

the studies of iron based superconductors[17, 27, 28] and it may be related to the strong spin fluctuation, which is beyond DFT calculation. We adopt the experimental parameters in the following calculation unless otherwise specified.

The band structure, the density of states(DOS) and Fermi surfaces for  $K_2Cr_3As_3$  have been calculated in Ref.29. Our results as shown in Appendix A are similar to their calculations. In general, the 3d states of Cr are located from -2.5 eV to 2.0 eV and the states near the Fermi level are mainly attributed to Cr  $d_{z^2}$ ,  $d_{xy}$  and  $d_{x^2-y^2}$  orbitals. The As 4p states mainly lie 1.0 eV below the Fermi level and hybridize strongly with the Cr 3d states. Along  $k_z$  direction, the bands are very dispersive due to the strong coupling between d orbitals along z direction. The bands attributed to Cr2  $d_{xy}$  and  $d_{x^2-y^2}$  orbitals are very close to half-filling. As the separation between chains is large, the inplane band dispersion is very small but not negligible. However, we want to point out an important feature that is ignored in Ref.29. Cr1 ions have more d electrons than Cr2 ions, which is consistent with analysis from the crystal structure. We will show later that this difference also results in different magnetic moments at Cr1 and Cr2 sites in magnetic states.

The band structure of  $Rb_2Cr_3As_3$ , shown also in Appendix A, shares many common features with that of  $K_2Cr_3As_3$ , but they also differ in some details. As the radius of Rb is bigger than K, Cr1As layer can get more electrons and  $d_{xy}$  and  $d_{x^2-y^2}$  bands of Cr1 are fully occupied. Meanwhile, the  $d_{xy}$  and  $d_{x^2-y^2}$  bands of Cr2 are much less occupied. It leads to great difference between the 3D Fermi surfaces of the two materials. Another difference is that there is an additional electron Fermi surface near  $A(0, 0, \pi)$  point in  $Rb_2Cr_3As_3$ , which is attributed to  $d_{xy}$  and  $d_{x^2-y^2}$  orbitals of Cr2. Finally the  $d_{xz}$  and  $d_{yz}$  orbitals are much close to the Fermi level in  $Rb_2Cr_3As_3$ . The calculated  $N(E_F)$  in  $K_2Cr_3As_3$  ( $Rb_2Cr_3As_3$ ) is 8.76(9.13)  $\text{eV}^{-1}/\text{f.u.}$ . The calculated Pauli susceptibility and specific heat coefficient are  $\chi_0 = 2.83(2.95) \times 10^{-4}$  emu/mol and  $\gamma = 20.7(21.5)$  mJ/( $K^2$  mol). The calculated  $\gamma$  is about only one third of the experimental value in  $K_2Cr_3As_3$ , suggesting strong correlation in these systems.

Now we focus on the magnetic properties. We consider four possible collinear magnetic states, the paramagnetic state (PM), the ferromagnetic (FM) state, the interlayer antiferromagnetic (AFM) state and the up-up-down-down ( $\uparrow\uparrow\downarrow\downarrow$ ) magnetic state. Due to strong magnetic frustration, we also consider two additional co-planar antiferromagnetic states: all-in magnetic state (Fig.1(b)) and in-out magnetic state (Fig.1(c)). We perform calculations with spin orbital coupling (SOC) and the calculated magnetic moments and the total relative energies of above magnetic states are summarized in Table II. The IOP state is the ground state in  $K_2Cr_2As_2$  ( $Rb_2Cr_2As_2$ ), with a large energy gain of 39(762) meV/cell relative to the PM state. The magnetic moments are 0.90(1.75) and 0.94(2.34)  $\mu_B$  on Cr1 and Cr2 sites, respectively. The initial FM state converges to a PM or AFM state, indicating that the interlayer magnetic coupling  $J_1'$  as indicated in Fig.1(d) is antiferromagnetic and relatively strong. In the AFM state, the energy gain is 25(486) meV/cell and the three magnetic moments at Cr1 or Cr2 site are different. It manifests that the intralayer

magnetic couplings among three Cr atoms  $J_1$  is AFM. Thus, strong magnetic frustration exists in  $A_2Cr_3As_3$ . Our results are different from those in Ref.[29] which missed to identify the IOP as the true magnetic ground state in their calculations. To confirm our results, we have performed all-electron calculations and find that relative energies and magnetic moments for collinear states are rather close to those in Table II.

The IOP state gains energy rapidly and becomes very robust if we include additional  $U$ , the onsite electron-electron correlation. The results from GGA+ $U$  calculations are given in Table III. The IOP state in  $K_2Cr_2As_2(Rb_2Cr_2As_2)$  has a large energy gain of 392(466) meV/cell relative to the AFM state. The magnetic moments are greatly enhanced to 2.49(2.76) and 2.56(2.92)  $\mu_B$  on Cr1 and Cr2 sites as well. It is also important to note that the magnetism is always found to be stronger in  $Rb_2Cr_3As_3$  than in  $K_2Cr_3As_3$ . In the presence of  $U$ , as the calculation can be converged for different magnetic states, we can extract the magnetic exchange parameters from their energy differences[30]. In the GGA+ $U$  calculations, the local magnetic moments on Cr are very close to each other. Thus, we can extract the magnetic exchange parameters from their energy differences within the Heisenberg Model. The energies contributed by magnetic interactions in these five magnetic states per cell are written as,

$$\begin{aligned} E_{FM}/S^2 &= 6J_1 + 12J'_1 + 6J_2, \\ E_{AFM}/S^2 &= 6J_1 - 12J'_1 + 6J_2, \\ E_{\uparrow\uparrow\downarrow}/S^2 &= 6J_1 - 6J_2, \\ E_{all-in}/S^2 &= -3J_1 + 6J'_1 + 6J_2, \\ E_{in-out}/S^2 &= -3J_1 - 6J'_1 + 6J_2. \end{aligned} \quad (1)$$

Using the relative energies and the above equations, we can obtain four equations. But there are only three exchange parameters. For this overdetermined system of equations, we can obtain these parameters by using a least-squares technique. The estimated exchange couplings are  $J_1 = 0.090$  eV/S<sup>2</sup>,  $J'_1 = 0.060$  eV/S<sup>2</sup>,  $J_2 = -0.010$  eV/S<sup>2</sup> for  $K_2Cr_3As_3$  and  $J_1 = 0.075$  eV/S<sup>2</sup>,  $J'_1 = 0.045$  eV/S<sup>2</sup>,  $J_2 = -0.020$  eV/S<sup>2</sup> for  $Rb_2Cr_3As_3$  in the GGA+ $U$  calculations. The NN exchange couplings  $J_1$  and  $J'_1$  are strongly AFM. However, the next NN exchange coupling  $J_2$  is ferromagnetic. The IOP state saves energy from all these effective exchange couplings.

Fig.2(a) and (b) show the calculated band structure and DOS in the IOP magnetic state of  $K_2Cr_3As_3$ . The material remains metallic in the presence of the static magnetic order. The bands near the Fermi level split due to SOC and magnetic order but the orbital characters have little changes compared with those in PM state. This splitting depends on orbital characters of the bands: it is larger for  $d_{xy}, d_{x^2-y^2}$  and  $d_{xz}, d_{yz}$  bands than for  $d_{z^2}$  bands.

As the size of Rb atoms is much larger than the size of K atoms, the stronger magnetism in  $Rb_2Cr_3As_3$  than in  $K_2Cr_3As_3$  suggests that applying pressure can suppress magnetic fluctuations. To simulate the effect of pressure, we investigate the magnetism as a function of the lattice constant  $c$ . Fig.3(a) shows the calculated magnetic moments and relative energies of the IOP magnetic state(relative to PM state) as a function of  $c$ . As the decrease of  $c$ , which is equivalent

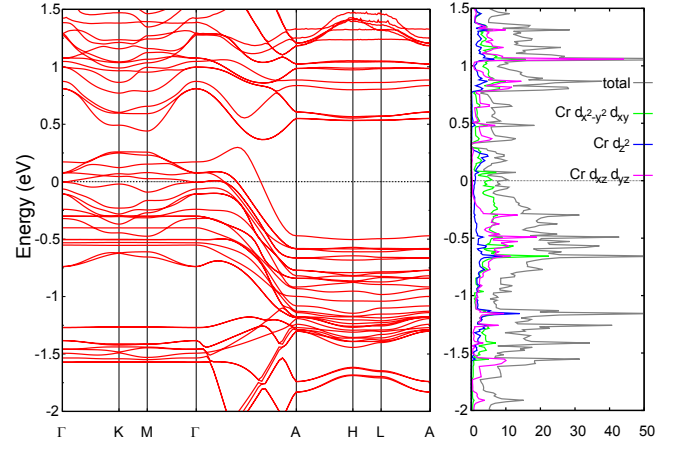


FIG. 2: Band structure and DOS for  $K_2Cr_3As_3$  in in-out co-planar (IOP) magnetic state.

TABLE II: The total energies for different magnetic states of  $A_2Cr_3As_3$ . They are given relative to the total energy of the PM state and the unit is meV/cell. The magnetic moments are given in  $\mu_B$ .

$A_2Cr_3As_3$		relative energy (meV/cell)	$M_{Cr1}$	$M_{Cr2}$
A=K	PM	0	0	0
	FM	to PM		
	AFM	-25	0.43	0.53
	$\uparrow\uparrow\downarrow$	to PM		
	all-in	-3(to in-out)	0.06	0.35
	in-out	-39	0.90	0.94
A=Rb	PM	0	0	0
	FM	-589(to AFM)	0.40	2.29
	AFM	-486	1.26	2.35
	$\uparrow\uparrow\downarrow$	-525	0.01	1.83
	all-in	-594(to in-out)	0.34	2.15
	in-out	-762	1.75	2.34

to the increase of pressure, the magnetic moments decrease, as well as the energy gains. When  $c = 4.06$  Å, the energy gain reaches zero, indicating the vanish of IOP magnetic orders. We also directly calculate the pressure effect using the GGA+ $U$  calculation. Consistent results are obtained as shown in Fig.3(b). These results allow us to conjecture a phase diagram of these new superconductors similar to the one shared by many Q2D unconventional superconductors as sketched in Fig.4(a). The non-Fermi liquid behaviors observed in experiments can be naturally explained as a result of strong magnetic fluctuations in the critical region.

We can construct a minimum effective Hamiltonian to describe the magnetism for a Q1D chain in  $A_2Cr_3As_3$  with the above mentioned magnetic exchange couplings. The Hamiltonian is

$$\begin{aligned} H_M &= J_1 \sum_{i,\alpha\beta} \mathbf{S}_{i\alpha} \cdot \mathbf{S}_{i\beta} + J'_1 \sum_{\langle ij \rangle, \alpha\beta} \mathbf{S}_{i\alpha} \cdot \mathbf{S}_{j\beta} \\ &+ J_2 \sum_{\langle\langle ij \rangle\rangle, \alpha\beta} \mathbf{S}_{i\alpha} \cdot \mathbf{S}_{j\beta}, \end{aligned} \quad (2)$$

TABLE III: The total energies for different magnetic states of  $A_2Cr_3As_3$  with GGA+U calculations. They are given relative to the total energy of the AFM state and the unit is meV/cell. The magnetic moments are given in  $\mu_B$ .

$A_2Cr_3As_3$		relative energy (meV/cell)	$M_{Cr1}$	$M_{Cr2}$
A=K	FM	+1495	2.47	2.58
	AFM	0	2.48	2.41
	$\uparrow\uparrow\downarrow\downarrow$	+854	1.50	2.44
	all-in	+311	2.35	2.43
	in-out	-392	2.49	2.56
A=Rb	FM	+1045	2.09	2.84
	AFM	0	2.70	2.97
	$\uparrow\uparrow\downarrow\downarrow$	+792	2.72	2.90
	all-in	+184	2.90	2.96
	in-out	-466	2.76	2.92

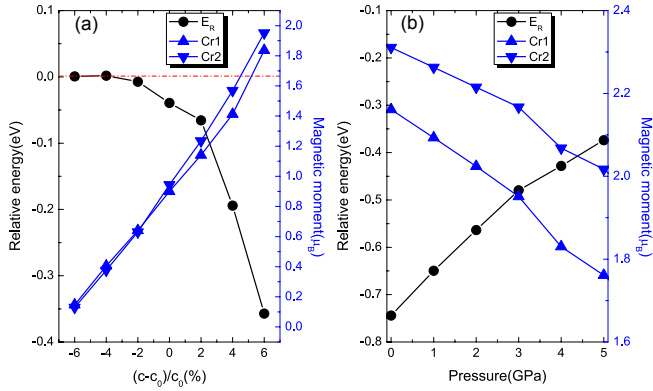


FIG. 3: The relative energies and magnetic moments as function of lattice constant  $c$  (a) and pressure (b). In the case of pressure, we performed structure relaxation and GGA+U calculations.

where  $\alpha, \beta$  label sublattices and  $\langle ij \rangle$  and  $\langle\langle ij \rangle\rangle$  denote the NN and next NN pairs. With  $J_1, J'_1$  being AFM and  $J_2$  being FM,  $H_M$  has the IOP magnetic ground state as a classical spin model or in the large S-limit. The magnetic excitations can be calculated by employing the Holstein-Primakoff transformation within the linear spin-wave approximation. As the 1D chain described by  $H_M$  has a  $C_{3v}$  symmetry with six Cr atoms in the unit cell, there must be three acoustic and three optical spin excitations. Each of these three modes must be composed of one  $A_1$  and two degenerated  $E$  modes. The detailed analytic results of the spin waves are given in Appendix B. A typical spin wave spectrum is plotted in Fig.4(b). The acoustic spin wave dispersion shows a linear dependence with small  $k_z$ , which indicates the AFM nature of the magnetic exchange couplings.

Although there is no direct experimental measurement on magnetic properties in these materials, the magnetic exchange coupling parameters obtained from our calculation are consistent with recent experimental measurements in CrAs[31], a MnP-type orthorhombic crystal structure and also a superconductor under pressure[32]. The magnetic order in CrAs is a double helimagnetic structure. Along the one-dimensional helimagnetic structure, the measurements have shown that it

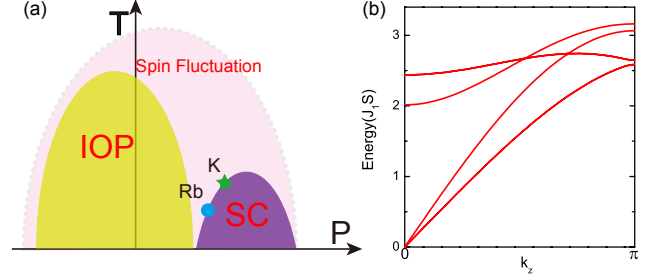


FIG. 4: (a) The conjectured phase diagram with pressure of  $A_2Cr_3As_3$ . (b) The calculated spin-wave dispersion of  $A_2Cr_3As_3$  along  $k_z$  direction, with  $J'_1=0.7J_1$  and  $J_2=-0.15J_1$ .

is AFM between two NN Cr atoms that has a Cr-As-Cr angle  $\sim 72^\circ$  and FM between two next NN Cr atoms that has a Cr-As-Cr angle  $\sim 123^\circ$ . These two magnetic exchange couplings in CrAs resemble  $J_1(J'_1)$  and  $J_2$ . It is interesting to note that the exchange couplings between two Cr atoms are against the simple Goodenough-Kanamori-Anderson (GKA) rules which would suggest opposite signs for  $J_1(J'_1)$  and  $J_2$ . Such a violation suggests that multi-magnetic mechanisms may work together in CrAs based structures and  $J_2$  may include significant contribution from the double-exchange mechanism since the average valence of Cr atoms in  $A_2Cr_3As_3$  is 2.3.

We have ignored the Dzyaloshinskii-Moriya (DM) term that can be induced by spin orbital couplings in the absence inversion center between two Cr atoms. In CrAs, the DM term is important in determining the incommensurate wavevector in the double helimagnetic structure. However, in  $A_2Cr_3As_3$ , the effect of the DM is greatly reduced as the Cr atoms form a tight octahedral cluster. This is consistent with our calculation results that magnetic moments tend to be in the  $xy$  plane.

Our results suggest that similar to cuprates and iron-based superconductors, the magnetic fluctuations are responsible for the superconductivity in  $A_2Cr_3As_3$ . If this is the case, it is interesting to ask what type of pairing is favored from the specific magnetic fluctuations predicted here. We argue that the favorite pairing is likely to be spin-triplet pairing from the magnetic fluctuations. As shown in Appendix A, the Cr1 and Cr2 atoms make major contributions to different bands near the Fermi level. Thus, as the pairing is expected to be dominated by the intra-band pairing, in the real space picture the majority pairing takes place within each sublattice that only contains one type of Cr atoms. The effective magnetic fluctuations within each sublattice along the chain direction connected by  $J_2$  are clearly FM from the above results. Therefore, if we ignore the parity breaking caused by alkaline atoms, the pairing from the magnetic fluctuations is very likely to be a  $p$ -wave spin triplet as the correlation effect forbids any onsite pairing. If we consider that the pairing is determined by the local FM exchange coupling[33], the induced gap function,  $\Delta \propto \sin k_z$ , which should be characterized by line nodes on the Fermi surface in the  $k_z = 0$  plane in reciprocal space.

In summary, we predict the Q1D superconductors,  $A_2Cr_3As_3$ , are close to a novel in-out co-planar magnetic ordered state and share a typical phase diagram similar to those



of Q2D high temperature superconductors, cuprates and iron-based superconductors. The prediction qualitatively explains the non Fermi-liquid behaviors observed in these systems and suggests that the superconductivity in these systems are driven by electron-electron correlation effects. We also predict that  $T_c$  can be maximized in these systems by applying certain external pressure. The new materials can be an ideal Q1D system to understand the intimate relation between magnetism and superconductivity.

*Acknowledgments* We thank S. M. Nie and Q. Xie for the help on calculations. The work is supported by "973" program (Grant No. 2010CB922904, No. 2012CV821400 and No. 2015CB921300), the National Science Foundation of China (Grant No. NSFC-1190024, 11175248 and 11104339) and the Strategic Priority Research Program of CAS (Grant No. XDB07000000). We also want to note that the authors in[29] have checked our results and have acknowledged to us that they missed the IOP ground state.

- 
- [1] Jerome D, Mazaud A, Ribault M, and Bechgaard K 1980 Journal De Physique Lettres **41**, L95
  - [2] Wilhelm H, Jaccard D, Duprat R, Bourbonnais C, Jrome D, Moser J, Carcel C and Fabre J M 2001 Eur. Phys. J. B **21**, 175
  - [3] Armici J C , Decroux M, Fischer O, Potel M, Chevrel R, and Sergeant M 1980 Solid State Commun. **33**, 607
  - [4] Greenblatt M, McCarroll W H, Neifeld R, Croft M, and Waszczak J V 1984 Solid State Commun. **51**, 671
  - [5] Denlinger J D, Gweon G H, Allen J W, Olson C G, Marcus J, Schlenker C and Hsu L S 1999 Phys. Rev. Lett. **82**, 2540.
  - [6] Xu X *et al* 2009 Phys. Rev. Lett. **102**, 206602
  - [7] Mercure J F *et al* 2012 Phys. Rev. Lett. **108**, 187003
  - [8] Bao J K *et al* 2015 Phys. Rev. X **5**, 011013
  - [9] Tang Z T *et al* 2015 Phys. Rev. B **91**, 020506
  - [10] Lee P A, Nagaosa N, and Wen X G 2006 Rev. Mod. Phys. **78**, 17
  - [11] Johnston D C 2010 Adv. Phys. **59**, 803
  - [12] Mazin I I, Singh D J, Johannes M D, and Du M H 2008 Phys. Rev. Lett. **101**, 057003
  - [13] Cao C, Hirschfeld P J and Cheng H P 2008 Phys. Rev. B **77**, 220506
  - [14] Ma F J and Lu Z Y 2008 Phys. Rev. B **78**, 033111
  - [15] Dong J *et al* 2008 Europhys. Lett. **83**, 27006
  - [16] Yildirim T 2008 Phys. Rev. Lett. **101**, 057010
  - [17] Yin Z P, Lebgue S, Han M J, Neal B P, Savrasov S Y and Pickett W E 2008 Phys. Rev. Lett. **101**, 047001
  - [18] Ma F J, Ji W, Hu J P, Lu Z Y and Xiang T 2009 Phys. Rev. Lett. **102**, 177003.
  - [19] Dai P C, Hu J P and Dagotto E 2012 Nat. Phys. **8**, 709
  - [20] Kresse G and Hafner J 1993 Phys. Rev. B **47**, 558.
  - [21] Kresse G and Furthmuller J 1996 Comput. Mater. Sci. **6**, 15
  - [22] Kresse G and Furthmuller J 1996 Phys. Rev. B **54**, 11169.
  - [23] Perdew J P, Burke K and Ernzerhof M 1996 Phys. Rev. Lett. **77**, 3865
  - [24] Monkhorst H J and Pack J 1976 Phys. Rev. B **13**, 5188
  - [25] Dudarev S L, Botton G A, Savrasov S Y, Humphreys C J and Sutton A P 1998 Phys. Rev. B **57**, 1505
  - [26] Mazin I I 2007 Phys. Rev. B **75**, 094407
  - [27] Singh D J 2008 Phys. Rev. B **78**, 094511
  - [28] Mazin I I, Johannes M D, Boeri L, Koepernik K and Singh D J 2008 Phys. Rev. B **78**, 085104
  - [29] Jiang H, Cao G H and Cao C 2014 arXiv: 1412.1309
  - [30] Wu X X, Cai Y X, Xie Q, Weng H M, Fan H and Hu J P 2012 Phys. Rev. B **86** 134413
  - [31] Shen Y *et al* 2014 arXiv:1409.6615
  - [32] Wu W *et al* 2014 Nat. Commun. **5**, 5508
  - [33] Hu J P and Ding H 2012 Sci. Rep. **2**, 381

### Appendix A: Electronic structures of $A_2Cr_3As_3$

The band structure and density of states(DOS) for  $K_2Cr_3As_3$  with experimental structural parameters are shown in Fig.5 (a) and (b),(c), respectively. From the band structure and DOS, we find that Cr1 ions have more  $d$  electrons than Cr2 ions, which is consistent with analysis from the crystal structure. It will lead to different magnetic moments at Cr1 and Cr2 sites in magnetic states. The Fermi surfaces are shown in Fig.7(a), which are similar to those in Ref.29. The band structure and DOS for  $Rb_2Cr_3As_3$ , shown in Fig.6, are similar to those of  $K_2Cr_3As_3$ . The main difference is that the 3D Fermi surface is quite different from that of  $K_2Cr_3As_3$  and there is an additional electron Fermi surface near  $A(0, 0, \pi)$  point, as shown in Fig.7(b).

### Appendix B: Spin excitations

The model of Cr octahedral clusters is shown in Fig.8. The magnetic excitations in the effective magnetic Hamiltonian, Eq.2, for  $A_2Cr_3As_3$  can be calculated by using the Holstein-

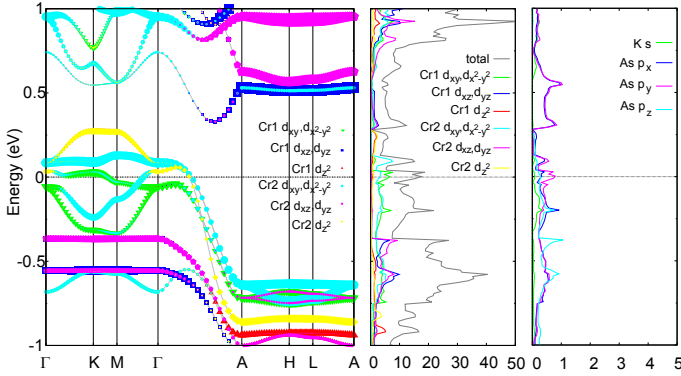


FIG. 5: Band structure and DOS of  $K_2Cr_3As_3$  with experimental parameters in the paramagnetic state.

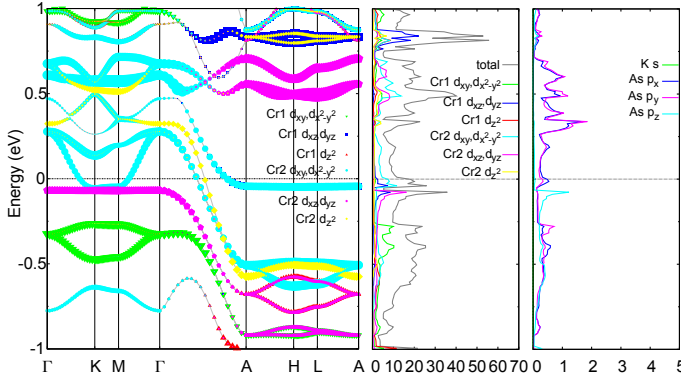


FIG. 6: Band structure and DOS of  $Rb_2Cr_3As_3$  with experimental parameters in the paramagnetic state.

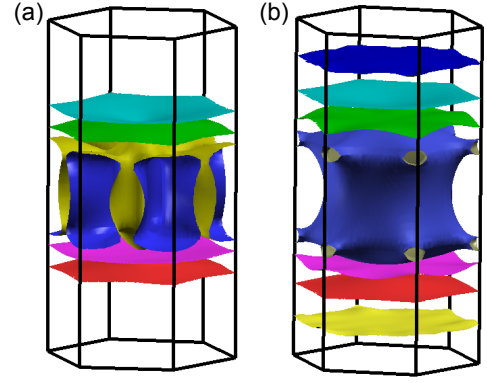


FIG. 7: Fermi surfaces of  $K_2Cr_3As_3$  (a) and  $Rb_2Cr_3As_3$  (b) with experimental parameters in the paramagnetic state.

Primakoff transformation,

$$\begin{aligned} S_{\alpha i}^+ &= \sqrt{2S - a_{\alpha i}^\dagger a_{\alpha i} a_{\alpha i}}, \\ S_{\alpha i}^- &= a_{\alpha i}^\dagger \sqrt{2S - a_{\alpha i}^\dagger a_{\alpha i}}, \\ S_{\alpha i}^z &= S - a_{\alpha i}^\dagger a_{\alpha i}, \end{aligned} \quad (B1)$$

where  $\alpha$  labels sublattice and  $\alpha = (1, 2, 3, 4, 5, 6)$  and  $a_{\alpha i}$  is a bosonic operator. Then, keeping only the linear terms and using Fourier transformation, the magnetic Hamiltonian can be expressed as,

$$\begin{aligned}
H_M = & \sum_k H_0(1,2) + H_0(2,3) + H_0(3,1) + H_0(4,5) + H_0(5,6) + H_0(6,4) \\
& + \sum_k H_1(1,4) + H_1(1,6) + H_1(2,4) + H_1(2,5) + H_1(3,5) + H_1(3,6) \\
& + \sum_k H_2(1,1) + H_2(2,2) + H_2(3,3) + H_2(4,4) + H_2(5,5) + H_2(6,6),
\end{aligned} \tag{B2}$$

$$H_0(1,2) = \frac{SJ_1}{4}(a_{1k}^\dagger a_{2k} + a_{1k} a_{2k}^\dagger) + \frac{SJ_1}{2}(a_{1k}^\dagger a_{1k} + a_{2k}^\dagger a_{2k}) - \frac{3}{4}SJ_1(a_{1k}^\dagger a_{2-k}^\dagger + a_{1k} a_{2-k}) - \frac{1}{2}NJ_1S^2, \tag{B3}$$

$$\begin{aligned}
H_1(1,4) = & \frac{SJ'_1}{2}\cos\left(\frac{k_z}{2}\right)(a_{1k}^\dagger a_{4k} + a_{4k}^\dagger a_{1k}) - \frac{3}{2}SJ'_1\cos\left(\frac{k_z}{2}\right)(a_{1k} a_{4-k} + a_{1k}^\dagger a_{4-k}^\dagger) \\
& + SJ'_1(a_{1k}^\dagger a_{1k} + a_{4k}^\dagger a_{4k}) - J'_1NS^2,
\end{aligned} \tag{B4}$$

$$H_2(1,1) = 2SJ_2\cos(k_z)(a_{1k}^\dagger a_{1k}) - 2SJ_2\cos(k_z)(a_{1k}^\dagger a_{1k} + a_{1k}^\dagger a_{1k}) + J_2NS^2. \tag{B5}$$

In the basis  $\Phi^\dagger(k) = (a_{1k}^\dagger, a_{2k}^\dagger, a_{3k}^\dagger, a_{4k}^\dagger, a_{5k}^\dagger, a_{6k}^\dagger, a_{1-k}, a_{2-k}, a_{3-k}, a_{4-k}, a_{5-k}, a_{6-k})$ , the magnetic Hamiltonian is,

$$H_M = \frac{1}{2} \sum_k \Phi^\dagger(k) h(k) \Phi(k) - S(S+1)N(3J_1 + 6J'_1 - 6J_2), \tag{B6}$$

$$h(k) = \begin{pmatrix} A & B & B & D & 0 & D & 0 & C & C & E & 0 & E \\ B & A & B & D & D & 0 & C & 0 & C & E & E & 0 \\ B & B & A & 0 & D & D & C & C & 0 & 0 & E & E \\ D & D & 0 & A & B & B & E & E & 0 & 0 & C & C \\ 0 & D & D & B & A & B & 0 & E & E & C & 0 & C \\ D & 0 & D & B & B & A & E & 0 & E & C & C & 0 \\ 0 & C & C & E & 0 & E & A & B & B & D & 0 & D \\ C & 0 & C & E & E & 0 & B & A & B & D & D & 0 \\ C & C & 0 & 0 & E & E & B & B & A & 0 & D & D \\ E & E & 0 & 0 & C & C & D & D & 0 & A & B & B \\ 0 & E & E & C & 0 & C & 0 & D & D & B & A & B \\ E & 0 & E & C & C & 0 & D & 0 & D & B & B & A \end{pmatrix}, \tag{B7}$$

$$A = J_1S + 2J'_1S - 2J_2S + 2J_2S\cos k_z, \tag{B8}$$

$$B = \frac{1}{4}J_1S, \tag{B9}$$

$$C = -\frac{3}{4}J_1S, \tag{B10}$$

$$D = \frac{1}{2}J'_1S\cos\left(\frac{k_z}{2}\right), \tag{B11}$$

$$E = -\frac{3}{2}J'_1S\cos\left(\frac{k_x}{2}\right). \tag{B12}$$

The spectrum of the spin wave is given in Fig.9, with  $J'_1 = 0.7J_1$ ,  $J_2 = -0.15J_1$ . In  $A_2Cr_3As_3$ , the bond lengths in Cr1As1 and Cr2As2 planes are different, which leads to different  $J_1$  couplings in Cr1As1 and Cr2As2 planes. Therefore,

we plot the spectrum of spin wave (Fig.4(b)) in the main text with  $J_{1Cr1} = J_1$ ,  $J_{1Cr2} = 0.9J_1$  and  $J'_1 = 0.7J_1$ ,  $J_2 = -0.15J_1$ . Compared with Fig.9, there are gaps on the Brillouin Zone boundary, indicating the intrinsic two sublattices.

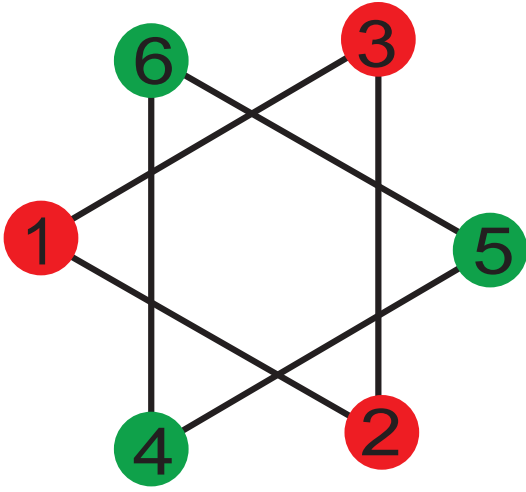


FIG. 8: Model of the Cr octahedral cluster in  $A_2Cr_3As_3$ .

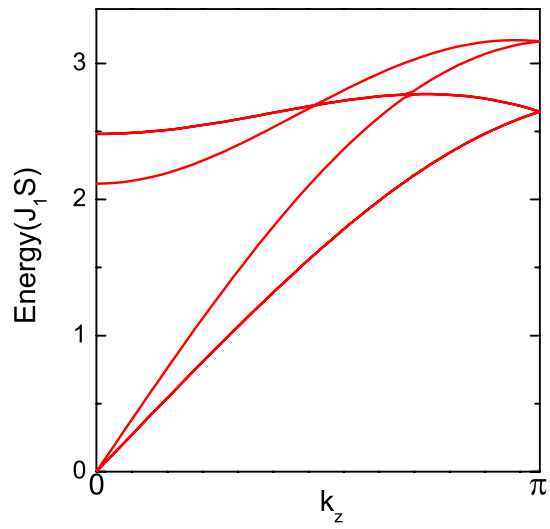


FIG. 9: The calculated spin-wave dispersion of  $K_2Cr_3As_3$  along  $k_z$  direction, with  $J_{1Cr1} = J_{1Cr2} = J_1$ ,  $J'_1 = 0.7J_1$  and  $J_2 = -0.15J_1$ .